Available online at www.sciencedirect.com

ScienceDirect

journal homepage: www.elsevier.com/locate/he

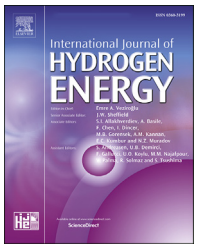

Numerical investigation of self-sustaining modes of 2D planar detonations under concentration gradients in hydrogen–oxygen mixtures

Qingguan Song, Yong Han[**], *Wei Cao*[*]

Institute of Chemical Materials, China Academy of Engineering Physics, Mianyang, Sichuan, 621999, China

HIGHLIGHTS

- Self-sustaining detonation modes in non-uniform mixtures are numerically studied.
- High-resolution codes with detailed chemical kinetics model are developed.
- Cellular structures, failure and re-initiation of detonations are characterized.
- Different concentration gradients produce different modes of detonation.

ARTICLE INFO

Article history:
Received 13 June 2020
Received in revised form
18 July 2020
Accepted 2 August 2020
Available online 22 August 2020

Keywords:
Self-sustaining mode of detonation
Concentration gradient
Weighted essentially non-oscillatory (WENO) scheme
Additive Runge-Kutta (ARK) scheme
Detailed chemical kinetic model
Hydrogen

ABSTRACT

Self-sustaining modes of detonations in non-uniform mixtures for hydrogen and oxygen are numerically studied. Concentration gradients are set vertical to the direction of detonation propagation, with equivalence ratios decreasing from rich values to lean ones. High-resolution codes based on the fifth-order weighted essentially non-oscillatory (WENO) scheme in spatial discretization and the 3rd-order Additive Runge-Kutta (ARK) schemes in time discretization, with detailed chemical kinetics model, are developed. Two-dimensional (2D) numerical simulations are conducted in a 2D planar geometry, non-uniform distributions are then precisely controlled as a function of width. The cellular structures and transmissions, failure and re-initiation mechanisms of detonation fronts are characterized. Results show that the low concentration gradient produces the multi-head mode of detonation with continuous adaptation of velocities and multicellular structures to local concentration. The high concentration gradient generates single-head mode with detonation re-initiation at channel walls produced by reflected transverse Mach waves. Specially, the intermediate distribution between the low and high concentration gradients induces an alternation mode between singe-head and multi-head detonations.

* *Corresponding author.*
** *Corresponding author.*
E-mail addresses: hanyong@caep.cn (Y. Han), weicao@caep.cn (W. Cao).
https://doi.org/10.1016/j.ijhydene.2020.08.014

Introduction

Self-sustaining gaseous detonation has complicated three-dimensional interactions between incident shock waves, Mach stems, transverse waves and channel boundaries, governing the detonation propagation [1]. Extensive studies have demonstrated that the self-sustaining modes of detonation can be divided into spinning mode, rectangular mode and diagonal mode depending on different boundary and initial conditions [2–8]. Among previous work, uniform combustible gas mixtures are usually studied. However, reactive mixtures often show spatial distributions of concentration and temperature, no matter for detonation engines or explosion accidents [9–15]. Specially, concentration gradients are considered as important reasons of the differences between predicted and measured dynamic detonation characteristics, and the self-sustaining detonation modes are important issues in detonation development and applications.

A mass of experimental and numerical studies has shown that the concentration gradient causes changes in global detonation structures, average velocities and cellular characteristics. Thomas et al. [16] discussed the influence of concentration gradients parallel to pipeline axis upon the propagating behavior of detonation waves, and observed the quenching and re-initiating behavior for different concentration gradients, which was also analyzed by Vidal [17]. Prokhorov [18,19] systematically studied the effect of concentration gradients on the planar detonation front and average detonation velocity, and gave an approximation formula which describes the relationship between detonation properties and concentration gradients. Boulal et al. [20] experimentally investigated the dynamic behavior of detonations with horizontal concentration gradients. Lieberman et al. [21] experimentally found that the detonation front was bended due to the propagation through non-uniform ethylene–oxygen (C_2H_4–O_2) mixtures. Ishii et al. [22] gave experimental results and theoretical explanation of cellular structures and declined fronts under different vertical concentration gradients. Ettner and Vollmer et al. [23–25] numerically studied the flame acceleration, deflagration to detonation transition and subsequently detonation wave propagation in mixtures with different concentration gradients. Kessler et al. [26] found that the activation energy and tube width had a significant effect on the instability and the extinction probability of detonations with vertical concentration gradients. Grune et al. [27] investigated the detonation waves propagation in semi-confined layers of hydrogen–air (H_2–air) mixtures with concentration gradients, and found that the detonation in a system with transversal gradient of reactivity does not follow real detonation cell sizes corresponding to local concentration because the process is driven by the mixture of highest reactivity. Then, involving the region of lower reactivity, an overdriven detonation propagates with cell sizes much lower than in a uniform mixture of the same concentration. Wang et al. [28] and Azadboni et al. [29] numerically studied the effect of concentration gradients on deflagration-to-detonation transition in H_2–air mixtures, and found that transverse concentration gradients can either strengthen or weaken flame acceleration, depending on the average hydrogen concentration. Based on abovementioned literatures, it has been observed that the concentration gradient mainly causes the change of the cell pattern and detonation velocity. However, rare quantitative description about self-sustaining modes is based on the actual distribution of concentrations. Boeck et al. [30,31] reported that a strong effect of vertical concentration gradients could be found on detonation propagation in H_2–air mixtures by means of high-speed shadowgraphy, OH imaging, pressure measurements, and soot foils. The single-head propagation with one strong transverse wave and multi-head propagation with a constant macroscopic front curvature over time and numerous weak transverse waves were investigated experimentally. Han et al. [32] investigated the role of transversal concentration gradients in detonation propagation. It was observed that the detonation instability, detonation velocity, and structure of detonation front could be changed by concentration gradients. Significantly, they illustrated this phenomenon with detailed reaction model and displayed the detailed multi-dimensional detonation structure with different concentration gradients.

An inherent coupling mechanism of the reaction and shock for the detonations under concentration gradients still needs to be identified and deeply investigated. Although many simulations tried to reveal the underlying mechanism [24,26], the numerical results provided finite explanation for this problem due to simplification of the reaction model and limitation of the computational resource. Simplified chemical kinetics is often considered, e.g., single-step reaction model and two-step reaction model. It is usually acknowledged that the detonation includes an induction zone and exothermic reaction zone [1,2,4,6,33]. The single-step model gives a rather continuous reaction profile without a distinguishable induction zone, thus the detonation cannot be quenched if the growth time is large enough. The single-step model do not reproduce correctly the transient and ignition process in detonation dynamics [34], which are critical in mixtures with concentration gradients. The two-step reaction model including the induction step and exothermic step is able to describe quantitatively many phenomena of detonation [35–38], e.g. detonability limit and induction length. Considered as an extension of empirical model, the two-step model consists of more empirical parameters that need fitting according to experimental results. In fact, the real detonation reaction zone includes complicated chain-branching reactions, HO_2 and H_2O_2 reactions and chain-termination reactions for H_2–O_2 mixtures [39], the detailed reaction mechanism has advantages to describe the complicated interactions between shock and reaction [40–43]. Recognizing that detonations in non-uniform mixtures with equivalence ratios changing from rich fuel to lean one, namely the concentration gradients, depend strongly on the detailed reaction mechanism and their study is still insufficient, as substantiated by Oran et al. [44,45], the globally planar detonation in the inhomogeneous mixtures was undertaken by using detailed chemical reaction mechanism.

The aim of this work is to simulate physical phenomena and explain self-sustaining detonation modes with different concentration gradients in H_2–O_2 mixtures. Two-dimensional (2D) numerical parallel codes based on detailed reaction

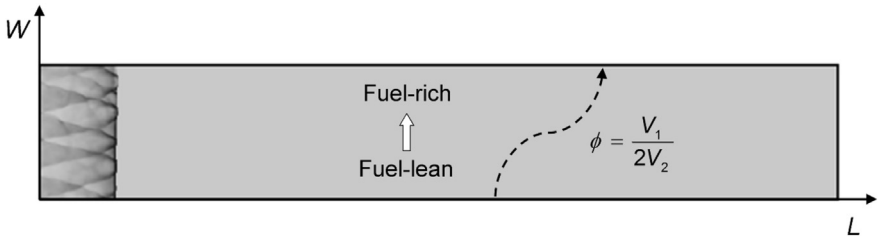

Fig. 1 – Calculation model: cellular detonation propagates toward the right, and concentration gradient is set in the unreacted gas.

mechanism enable us to observe the strong-coupled detonation front, shock-reaction coupling process and complicated transverse structure after detonation front. The multi-species reactive Euler equations and numerical method are presented first, and then results and discussions are followed.

Governing equation and numerical method

2D numerical simulations are conducted in a 2D planar channel with width (W_0) of 72 mm and length (L) of 2000 mm. Reactive flow Euler equations are used to describe the detonation propagation in H_2–O_2 system with multi species and detailed reactions as following:

$$\frac{\partial \boldsymbol{U}}{\partial t}+\frac{\partial \boldsymbol{F}(\boldsymbol{U})}{\partial x}+\frac{\partial \boldsymbol{G}(\boldsymbol{U})}{\partial y}=\boldsymbol{S}(\boldsymbol{U}) \tag{1}$$

$$\boldsymbol{U}=(\rho,\rho u,\rho v,\rho e,\rho Y_1,\ldots,\rho Y_{N-1})^{\mathrm{T}} \tag{2}$$

$$\boldsymbol{F}(\boldsymbol{U})=\left(\rho u,\rho u^2+p,\rho uv,\rho u(e+p/\rho),\rho uY_1,\ldots,\rho uY_{N-1}\right)^{\mathrm{T}} \tag{3}$$

$$\boldsymbol{G}(\boldsymbol{U})=\left(\rho v,\rho vu,\rho v^2+p,\rho v(e+p/\rho),\rho vY_1,\ldots,\rho vY_{N-1}\right)^{\mathrm{T}} \tag{4}$$

$$\boldsymbol{S}(\boldsymbol{U})=(0,0,0,0,\dot{\omega}_1,\ldots,\dot{\omega}_{N-1})^{\mathrm{T}} \tag{5}$$

where u and v are the fluid velocities in x and y directions in Cartesian coordinate, ρ is the density, p is the pressure ($p = \rho R_u T$, where R_u is universal gas constant and T is the temperature related through the ideal gas law), $Y_1 \cdots Y_{N-1}$ are mass fractions of species i (1 to N-1) in detailed chemical kinetics model [37].

The total energy per unit mass e is expressed as

$$e=h-\frac{p}{\rho}+\frac{(u^2+v^2)}{2} \tag{6}$$

where h is the total enthalpy per unit mass that can be calculated with temperature and mass fractions.

The reaction rate per unit mass $\dot{\omega}_i$ is given by

$$\dot{\omega}_i=W_i\sum_{m=1}^{20}\left(v_{mi}^{''}-v_{mi}^{'}\right)\times \mathrm{TB}\times\left(kf_m\prod_{i=1}^{N}\left(\frac{\rho_i}{W_i}\right)^{v_{mi}^{'}}-kb_m\prod_{i=1}^{N}\left(\frac{\rho_i}{W_i}\right)^{v_{mi}^{''}}\right) \tag{7}$$

where, $v_{mi}^{'}$ and $v_{mi}^{''}$ are reactant and product chemical stoichiometric coefficients of the i-th species in the m-th reaction. kf_m and kb_m are the forward and backward reaction rate constants of the m-th reaction. ρ_i and W_i are the density and molecular weight of the i-th species. TB is the index of the third body effect. The related reaction parameters in [25] are used.

Considering the strong discontinuity of detonation waves and strong time stiffness of detailed reactions, the 5th-order Weighted Essentially Non-Oscillatory (WENO) scheme [46] shown as Eq. (8) for spatial discretization, and the 3rd-order explicit-implicit Additive Runge-Kutta (ARK) scheme [47] as Eq. (9) for time discretization are applied to solve the Euler equations numerically.

$$\left(\frac{\partial \boldsymbol{U}}{\partial t}\right)_{i,j}=-\frac{1}{\Delta x}\left(\hat{\boldsymbol{F}}_{i+1/2}^{+}-\hat{\boldsymbol{F}}_{i-1/2}^{+}\right)-\frac{1}{\Delta x}\left(\hat{\boldsymbol{F}}_{i+1/2}^{-}-\hat{\boldsymbol{F}}_{i-1/2}^{-}\right)-\frac{1}{\Delta y}\left(\hat{\boldsymbol{G}}_{j+1/2}^{+}-\hat{\boldsymbol{G}}_{j-1/2}^{+}\right)-\frac{1}{\Delta y}\left(\hat{\boldsymbol{G}}_{j+1/2}^{-}-\hat{\boldsymbol{G}}_{j-1/2}^{-}\right) \tag{8}$$

$$\begin{cases}\boldsymbol{U}^{(i)}=\boldsymbol{U}^{(n)}+\boldsymbol{X}^{(i)}+(\Delta t)a_{ii}^{[I]}\boldsymbol{F}_s^{(i)},\boldsymbol{X}^{(i)}=(\Delta t)\sum_{j=1}^{i-1}\left(a_{ij}^{[E]}\boldsymbol{F}_{ns}^{(j)}+a_{ij}^{[I]}\boldsymbol{F}_s^{(j)}\right),i=2,\cdots,s+1\\ \boldsymbol{U}^{(n+1)}=\boldsymbol{U}^{(n)}+(\Delta t)\sum_{j=1}^{s}\left(b_j^{[E]}\boldsymbol{F}_{ns}^{(j)}+b_j^{[I]}\boldsymbol{F}_s^{(j)}\right)\end{cases} \tag{9}$$

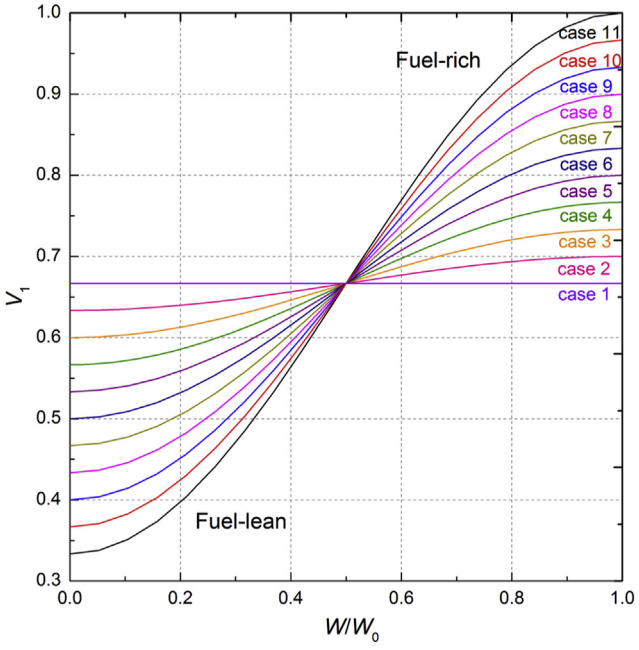

Fig. 2 – Volume fractions of hydrogen distribution as a function of the non-dimensional width W/W_0.

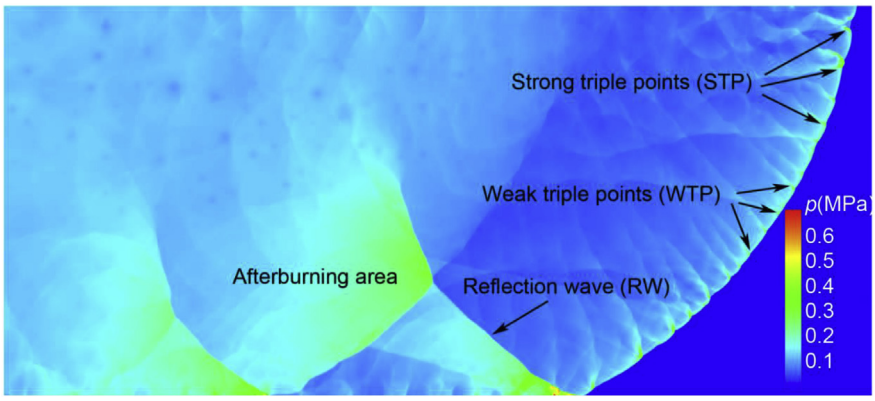

Fig. 3 – Detail structure of multi-head detonation fronts (pressure contour).

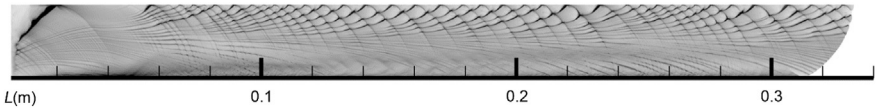

Fig. 4 – Cellular structures of self-sustaining detonations of the multi-head mode.

The 2D detonation simulation based on the detailed reaction mechanism requires an expensive computational cost. Since the Additive Runge-Kutta scheme is used to solve the stiffness of equations, the Jacobi matrix of the equation is calculated. Thus, the calculation scale is proportional to the square of the number of equations. The grid resolution of 0.01 mm is used to carry out following simulations. The MPI parallel platform [6] is used to divide the computational domain into N computational subdomains and the maximum number of subdomains in the simulations is about 1120.

The channel is filled with stratified hydrogen-oxygen mixtures. The left side is inlet and the right side is outflow. A resulted cellular detonation is set as the ignition zone in the left, as shown in Fig. 1. In the rest, the gas is stationary and its initial pressure and temperature is 7.0 kPa and 290 K, respectively.

To study systematically the influence of concentration gradients on detonations, we represent the equivalence ratio (ER) distributions by means of the function $\phi(W/W_0)$, with ϕ is the local ER value, W/W_0 is the non-dimensional position from the lower wall of the channel. Based on earlier results [22], the volume fraction of H_2 (V_1) can be expressed as:

$$V_1(W/W_0)=\frac{1}{2}[(V_1(1)-V_1(0))sin(\pi(W/W_0-0.5))+(V_1(1)+V_1(0))] \tag{10}$$

where $V_1(1)$ and $V_1(0)$ are the volume fractions at the upper and lower walls of the channel, respectively. Specially, the sum of $V_1(1)$ and $V_1(0)$ is identical for different cases, making the total concentrations unchanged. Then, the volume fraction of O_2 (V_2) can be expressed as $(1-V_1)$, and the ER distribution ϕ can be calculated as:

$$\phi = V_1/(2V_2) \tag{11}$$

Fig. 2 illustrates the eleven volume fractions of hydrogen distribution as a function of the non-dimensional width W/W_0 considered in this study. The ER distributions distinguish from one to another by the difference between highest and lowest

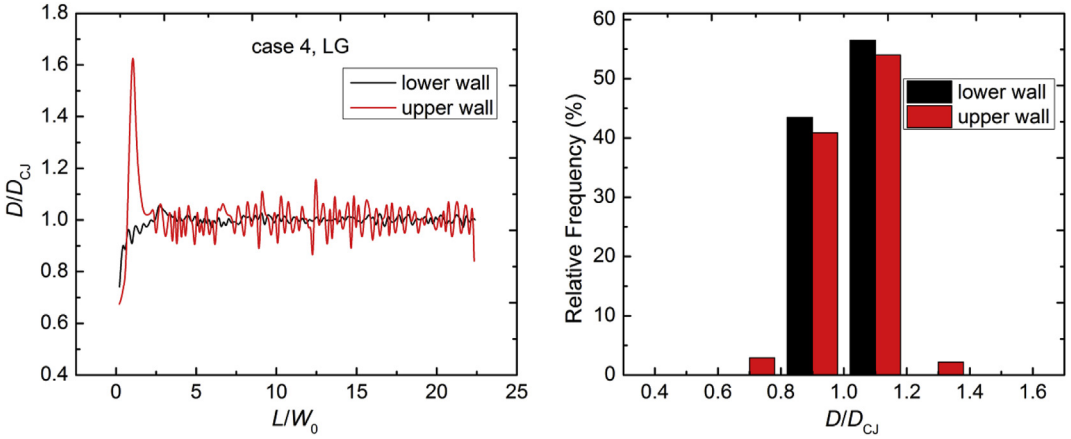

Fig. 5 – Normalized detonation velocities and histogram of the multi-head mode.

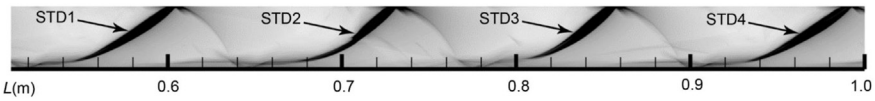

Fig. 6 – Cellular structures of self-sustaining detonations of the single-head mode.

ER values at the walls. Therefore, a concentration gradient exists vertically to the channel, resulting in different sustaining modes of detonation.

Results and discussions

Based on numerical simulations for different cases in Fig. 2, three distributions are classified to identify three self-sustaining detonation modes resulting from interaction of inclined detonation waves and channel walls:

(1) Multi-head mode: an inclined multicellular detonation wave is formed and the detonation velocity is changed due to the concentration at different widths. Specially, since the interaction of transverse waves from fuel-rich region, the overdriven detonation would occur in fuel-lean region. This mode is obtained with low gradient (LG) distributions (Fig. 2, cases 2–4).
(2) Single-head mode: the detonation is quenched at a certain distance and then is re-initiated by means of a strong transverse detonation wave generating from the lower wall, which agrees with earlier results of single-head mode obtained by Boeck et al. [30,31]. This dynamic is obtained with high gradient (HG) distributions (Fig. 2, cases 8–11).
(3) Alternative mode: the detonation firstly propagates as a multicellular wave with the increasing mean cell width. Then the detonation is suddenly quenched (shock-reaction decoupling) and the strong transverse detonation re-initiates the decoupling region later. After a while, the multicellular detonation appears again. This mode is obtained with the intermediate gradient (IG) distributions (Fig. 2, cases 5–7) located between the above two. However, this mode has not been observed in experiments.

The above classification can be applied to other combustible gas mixtures not just the specific one in this work. However, we must state that not all self-sustaining modes can be observed for any channel. We now detail each mode depending on the high-resolution numerical simulation.

Multi-head mode

Fig. 3 gives the detailed structure of detonation fronts with the multi-head mode for LG distribution (Fig. 2, case 4). It shows that the propagation of detonation waves is sustained by a collision between the transverse shock waves, which achieve the conversion of the Mach stem and the incident shock. The Mach stem regions have high pressure (~0.5 MPa) and the detonation front is not smooth, while the incident shock regions have relatively low pressure (~0.2 MPa) and detonation front is relatively smooth. This is because there are different reaction rates in the mixture shocked by the Mach stem and incident shock. With the propagation of detonation waves, the Mach stem turns into the incident shock as the intensity of the

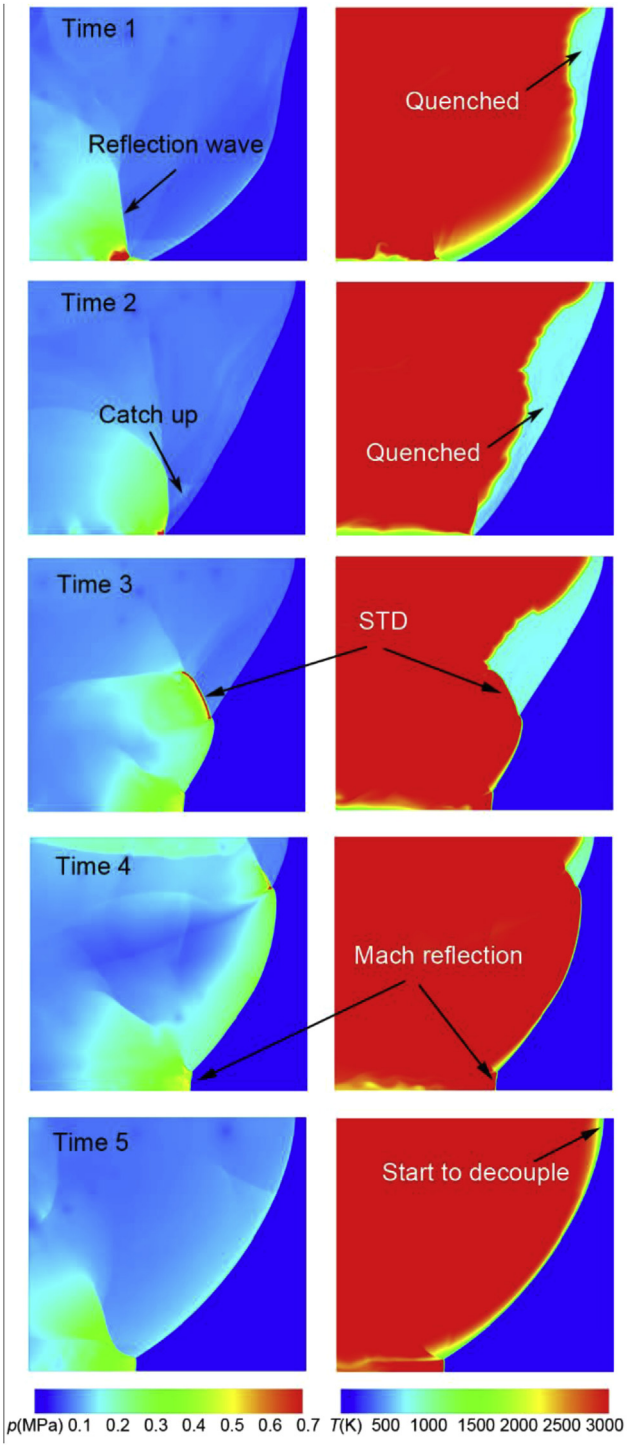

Fig. 7 – Formation progress of the STD1.

Mach stem is gradually weakened. Reaction zones are coupled with leading shocks and thereby detonations are self-sustaining.

The CJ detonation velocity can be calculated with the NASA CEA program for mixtures with different ER. The vertical concentration gradient causes a variation in detonation velocity D and hence leads to the inclination of the detonation front with respect to the vertical direction as shown in Fig. 3. We also observe that the regular reflection occurs at lower wall resulting from the interaction between the inclined detonation wave and channel wall. Due to the mixing of H_2 and O_2 after detonation fronts, an afterburning area with high pressure (~0.6 MPa) is formed and interacted with the first reflection wave, producing the second reflection wave. With the propagation of detonation waves, the distance between detonation front and afterburning area is basically unchanged, meaning that the self-sustaining mode cannot be influenced by the behind flowing state.

Fig. 4 shows cellular structures (i.e. history of maximum pressures) of detonations for case 4 in Fig. 2. The results show that the detonation front maintains multicellular waves structure during propagation in the channel. Specially, it is observed that the cellular structures evolve from a distinct pattern to an indistinct pattern. This is because that the pressure at triple points near upper wall (~0.6 MPa) is stronger than that near lower wall (~0.25 MPa) as shown in Fig. 3. It is indicated that the effect of triple points on self-sustaining detonation near lower wall is weak. It also can be seen from Fig. 4 that the mean cell width λ is varied as the detonation propagates, such as increasing from the value ~7 mm (at L ~ 240 mm) to ~ 15 mm (at L ~ 300 mm), less than the corresponding value for stoichiometric mixture $2H_2 + O_2$ (about 22–25 mm). Considering the mean cell width is proportional to the characteristic chemical length of the ZND reaction zone model [36], the existed concentration gradients slow down the rate of chemical reaction, thus the distance between the induced shock and CJ reaction front is larger with increasing concentration gradients than the uniform mixtures.

To demonstrate more detailed behavior for the multi-head mode, Fig. 5 shows the normalized detonation velocities (D/D_{CJ}) at lower and upper walls varied with normalized length (L/W_0) and their distribution histogram for case 4. Here and hereinafter, D_{CJ} refers in particular to the CJ detonation velocity of the stoichiometric mixture ($2H_2 + O_2$). It is observed that the detonation velocities at upper wall range from 0.7 D_{CJ} to 1.3 D_{CJ}, and the detonation velocities at lower wall range from 0.9 D_{CJ} to 1.1 D_{CJ}. Thus, the existence of concentration gradients makes detonation velocities near upper wall more fluctuant that those of lower wall, which is consistent with the distinct cellular structures near upper wall as shown in Fig. 4.

In summary, the detonation with the LG distribution propagates like that in the uniform mixture and is self-sustained by the collision of triple points.

Single-head mode

Fig. 6 illustrates cellular structures recorded in channel with HG distribution (Fig. 2, case 10). This concentration gradient

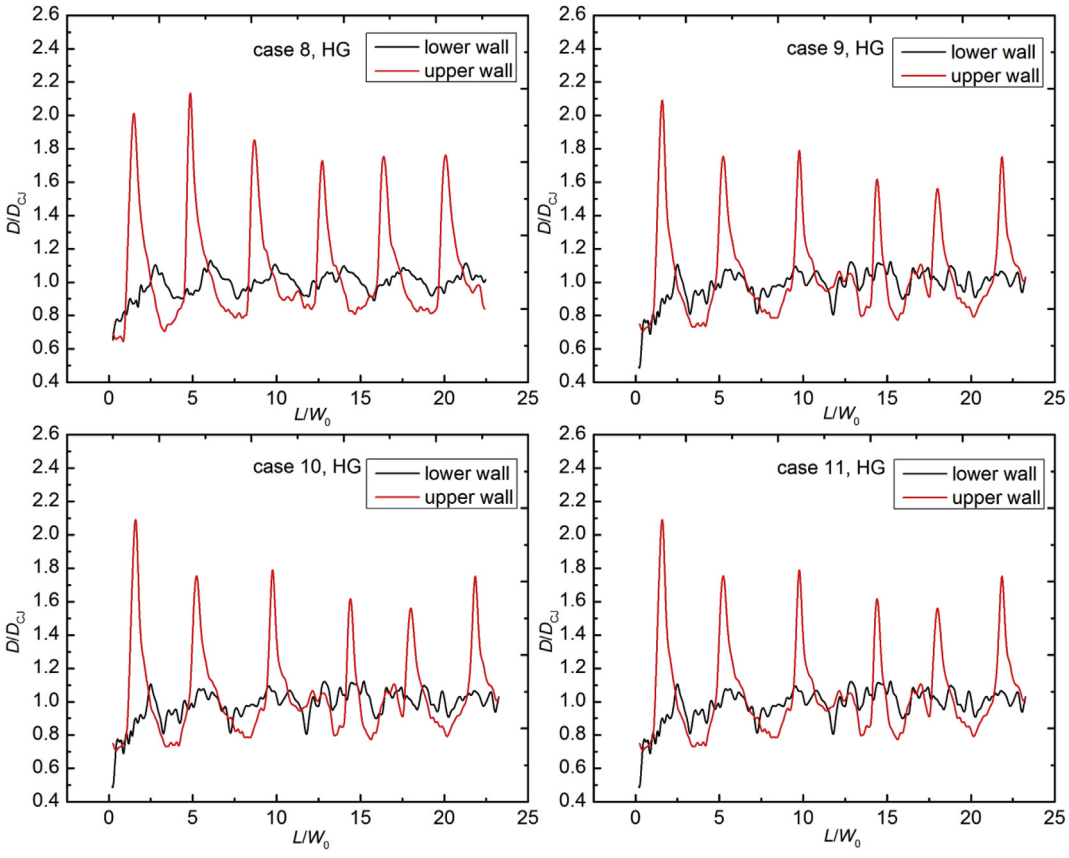

Fig. 8 – Normalized detonation velocities of the single-head mode for cases 8~11.

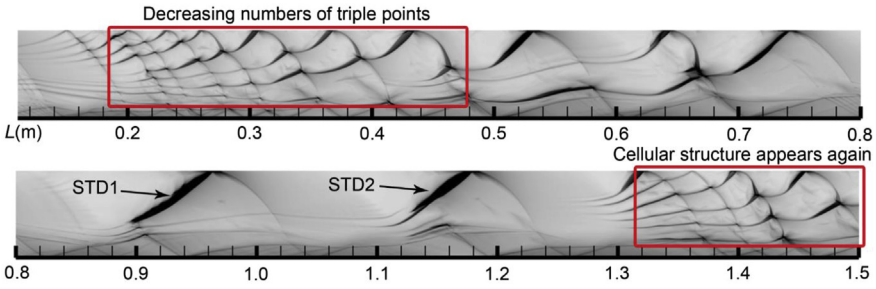

Fig. 9 – Cellular structures of self-sustaining detonations of the alternative mode.

leads to a single-head mode. Instead of cellular structures in Fig. 4, a periodical transverse track is formed. A sudden failure of detonation resulting from shock-reaction decoupling is observed, followed by a violent re-initiation originating from a strong transverse detonation (STD). In Fig. 6, the STD 1–4 arise at position L ~540, 670, 790, and 920-mm, and develop in the transverse direction. Specially, the cycles of the STD (~130 mm) are basically identical, indicating that this self-sustaining mode is stable for this concentration gradient. To illustrate the formation progress of the STD, Fig. 7 shows five sequences of detonation front structures recorded in STD 1 in Fig. 6.

At time 1 (t = 0.187 ms after initiation), the shock-reaction decoupling process near upper wall from $W/W_0 = 0.5$ to $W/W_0 = 1.0$ is observed and characterized by an increasingly large induction region without chemical reactions. A high-pressure region following the detonation front appears resulting from the regular reflection near the lower wall, similar to case 4 shown in Fig. 3.

At time 2 (t = 0.193 ms), the shock-reaction decoupling process at entire detonation fronts is observed and characterized by quenched reaction fronts separated from the induced shock waves. Considering the shock waves not sustained by chemical reaction is weakened, the following high-pressure region will catch up with the decoupled shock waves.

At time 3 (t = 0.210 ms), re-initiation in the fuel-rich layer near the lower wall with $W/W_0 \approx 0.05$ occurs and results in a local explosion due to high heat release, where overdriven detonation with high pressure (~0.63 MPa) appears.

At time 4 (t = 0.221 ms), considering the pressure (~0.12 MPa) and temperature (~1000 K) of the decoupled region are higher than those of un-shocked mixtures, the decoupled region can be easily initiated. We observe the formation and upward development of the STD with high velocity through the decoupled region, re-initiating the entire decoupling region. As shown in Fig. 6, the slope of the STD structure increases upward, which indicates that the STD is accelerating. We also observe the detonation front is strongly coupled after the STD. Mach reflections occur near the lower wall and the lengths of Mach stems maintain a fixed value. In non-Mach stem region, the detonation front is smooth without transverse structures.

At time 5 (t = 0.227 ms), the STD moves from fuel-lean layer (lower) to fuel-rich layer and creates entropy-vortex rolls behind it. The entropy-vortex rolls that transport the oxidizer into the fuel-rich layer enable a sufficient reaction. The STD disappears after it reaches the upper wall. The detonation front near upper wall starts to decouple, just similar to time 1, and the progress from time 1 to 5 will cycle.

Fig. 8 presents the effect of high concentration gradients (cases 8–11) on the detonation velocities of single-head mode detonations. It is observed that the detonation velocities at the lower wall distribute around 0.9–1.1 D_{CJ} with weak fluctuations for cases 8–11, and the period is irregular for cases 9–11. While for case 8–11, the detonation velocities at the upper wall fall closely to 0.8 D_{CJ}, then accelerate to about 1.8 D_{CJ} and subsequently decay again for the next cycle. Specially, the period of detonation velocity peaks at upper wall generated by the transverse detonation waves are basically the same when the detonation waves propagate with the single-head mode. This is because the transverse detonation waves propagate vertically and the average vertical concentration is basically the same under different concentration gradients.

The self-sustaining detonation with single-head mode develops in mixtures of high concentration gradients. The STD produced by the regular reflection plays a key role in this mode. Once the single-head mode appears and its period is determined by the channel width, it will be independent on the concentration gradients. We must emphasize that the detonation will be quenched without channel confinement for HG distributions.

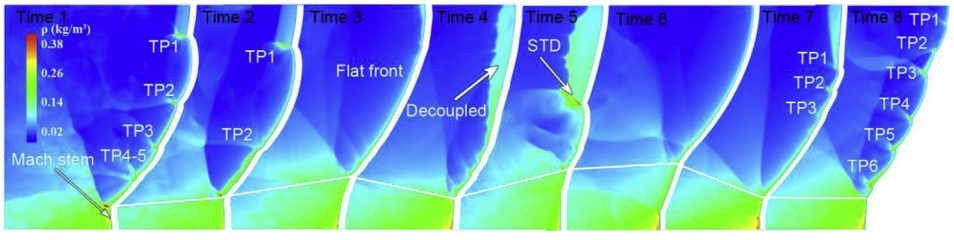

Fig. 10 – Propagation progress of self-sustaining detonations with the alternation mode.

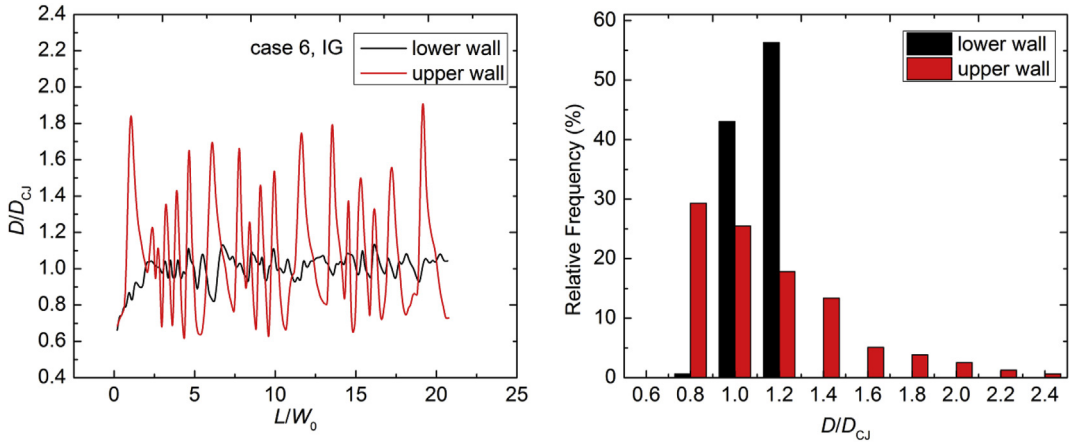

Fig. 11 – Normalized detonation velocities and histogram of the alternative mode for case 6.

Alternative mode

In order to get more insight into the re-initiation process, we have performed a set of numerical simulations of mixtures with IG distributions between the above LG and HG distributions, so that the detailed transformation mechanism between the multi-head mode and single-head mode can be investigated.

Fig. 9 gives cellular structures of self-sustaining detonations with an alternative mode (IG, Fig. 2, case 6). It is observed that the mean cell width increases from the leftmost part of the record. The cellular structures of detonations disappear at position L ~0.76 m. Like the single-head mode, the violent re-initiation of a STD at position L ~0.9 m is observed, however, in contrast with the single-head mode, the multicellular detonations appear at position L ~1.3 m. We also observe that the mean cell width increases after cell structures appear again, which is similar to the starting process. Thus, the detonations propagate with this self-sustaining mode are called the alternative mode, including both the multi-head mode and single-head mode. Fig. 10 shows eight sequences of detonation front structures recorded in Fig. 9.

At time 1 (t = 0.110 ms), the propagation of multicellular detonation fronts is observed and characterized by five triple points. The Mach reflection, instead of regular reflection, occurs at lower wall for this IG distribution. Similarly, we also observe a high-density region after the Mach stem.

At time 2 (t = 0.152 ms), we only observe two triple points. The number of triple points decreases as the detonations propagate forward.

At time 3 (t = 0.308 ms), triple points are vanished at entire detonation front. We only observe a smooth detonation front where the reactions and shock waves are coupled, meaning that the detonation is not quenched at this moment. Specially, a little decoupled region exists at the detonation front near the upper wall.

At time 4 (t = 0.322 ms), the shock-reaction decoupling process characterized by an increasingly-large reaction layer extends from upper wall to the majority of detonation front outside Mach stem.

At time 5 (t = 0.341 ms), the decoupled region is initiated by the high-pressure and high-temperature region behind the Mach reflection when it reaches the Mach stem. Similar to the process (time 3) in Section Single-head mode, we can also observe the STD generated at position $W/W_0 \approx 0.4$.

At time 6 (t = 0.445 ms), the detonation front is smooth without transverse structures from position $W/W_0 \approx 0.32$ to $W/W_0 = 1.0$. The detonation front structures at this time are basically similar to those at time 3, while the decoupled region is not observed.

At time 7 (t = 0.465 ms), three triple points generated on the multicellular detonation fronts are observed.

At time 8 (t = 0.483 ms), the number of triple points increases from three to six as detonation moves on. After time 8, similar detonation fronts as time 1 will emerge again for next cycle.

Fig. 11 shows the variation of detonation velocities at lower and upper walls with normalized length (L/W_0) and their histogram for case 6. The detonation velocities at the lower wall range from 0.9 to 1.1 D_{CJ} without obvious periodicity, which is like those of the multi-head mode for case 4. The detonation velocities at the upper wall range from 0.7 to 1.9 D_{CJ}, and their fluctuation range is like that of the single-head mode for cases 8–11, but the detonation velocity peaks for case 6 appear aperiodically. Therefore, the self-sustaining mode under IG distribution is unstable.

In summary, the self-sustaining mode under IG distribution, which is called the alternative mode, is unstable. This mode combines the multi-head mode with the single-head mode. The triple points or the strong transverse detonations generated by Mach reflections play a key role in the detonation propagation.

Conclusions

In this work, a numerical investigation into self-sustaining detonation modes in mixtures of H_2 and O_2 with concentration gradients, which are vertical to the detonation propagation, was presented. Eleven concentration gradients are

chosen and varied from fuel-lean concentrations near the lower wall to fuel-rich concentrations near the upper wall.

Based on numerical results, self-sustaining detonation modes are classified into three categories, i.e. the multi-head mode with triple points in case of low concentration gradients, the single-head mode with the strong transverse detonations in case of high concentration gradients, and the alternative mode with combination of triple points and strong transverse detonations in case of intermediate concentration gradients. Specially, the existence of high concentration gradients can completely change the self-sustaining detonation modes. For high concentration gradients, the strong transverse detonations play a key role in the detonation propagation. Once the single-head mode appears, its period is determined by the channel width and is independent on the concentration gradients.

Due to the interaction of inclined detonation waves and channel walls, the regular reflection or Mach reflection appears depending on the inclined angle of detonation, which makes a huge difference on the self-sustaining mode. For the regular reflection, a high-pressure and high-temperature region is generated behind the detonation front, which has no effect on the self-sustaining mode. However, it will catch up with the detonation front, and then initiate the shocked domain between the reaction flame and the induced shock. When the detonation starts to quench because of high concentration gradients, a strong transverse detonation generates suddenly, and re-initiates the whole quenched region. For the Mach reflection, the Mach stem, as a part of detonation front, has a higher pressure than the residual front sustained by collision of triple points. When the detonation front outside the Mach stem is quenched, the strong transverse detonation will also originate from Mach stem, and propagate in transverse direction.

More numerical work is still required to better understand the detailed quenching and re-initiating process based on Navier-Stokes equations with viscous terms. Considering the detailed reaction mechanism and the implicit-explicit schemes used, the computational scale will be so tremendous that we cannot afford for it now if the Navier-Stokes equations are applied in this work.

Declaration of competing interest

The authors declare that they have no known competing financial interests or personal relationships that could have appeared to influence the work reported in this paper.

Acknowledgments

This work was supported by the National Key R&D Program of China [grant no. 2017YFC0804700], and the Innovation Project of Innovation and Development Foundation of CAEP [grant no. CX2019009].

REFERENCES

[1] Lee JH. The detonation phenomenon. Cambridge: Cambridge University Press; 2008.
[2] Williams DN, Bauwens L, Oran ES. Detailed structure and propagation of three-dimensional detonations. Symp (Int) Combust 1996;26:2991–8. https://doi.org/10.1016/S0082-0784(96)80142-1.
[3] Tsuboi N, Eto K, Hayashi A. Detailed structure of spinning detonation in a circular tube. Combust Flame 2007;149:144–61. https://doi.org/10.1016/j.combustflame.2006.12.004.
[4] Dou H-S, Tsai HM, Khoo BC, Qiu J. Simulations of detonation wave propagation in rectangular ducts using a three-dimensional WENO scheme. Combust Flame 2008;154:644–59. https://doi.org/10.1016/j.combustflame.2008.06.013.
[5] Zhang B, Ng HD, Mével R, Lee JHS. Critical energy for direct initiation of spherical detonations in $H_2/N_2O/Ar$ mixtures. Int J Hydrogen Energy 2011;36:5707–16. https://doi.org/10.1016/j.ijhydene.2011.01.175.
[6] Wang C, Shu C-W, Han W, Ning J. High resolution WENO simulation of 3D detonation waves. Combust Flame 2013;160:447–62. https://doi.org/10.1016/j.combustflame.2012.10.002.
[7] Ivanov M, Kiverin A, Yakovenko I, Liberman MA. Hydrogen–oxygen flame acceleration and deflagration-to-detonation transition in three-dimensional rectangular channels with no-slip walls. Int J Hydrogen Energy 2013;38:16427–40. https://doi.org/10.1016/j.ijhydene.2013.08.124.
[8] Wu Y, Lee JH. Stability of spinning detonation waves. Combust Flame 2015;162:2660–9. https://doi.org/10.1016/j.combustflame.2015.03.021.
[9] Rigas F, Sklavounos S. Evaluation of hazards associated with hydrogen storage facilities. Int J Hydrogen Energy 2005;30:1501–10. https://doi.org/10.1016/j.ijhydene.2005.06.004.
[10] Brophy C, Hanson R. Fuel distribution effects on pulse detonation engine operation and performance. J Propul Power 2006;22:1155–61. https://doi.org/10.2514/1.18713.
[11] Rankin BA, Richardson DR, Caswell AW, Naples AG, Hoke JL, Schauer FR. Chemiluminescence imaging of an optically accessible non-premixed rotating detonation engine. Combust Flame 2017;176:12–22. https://doi.org/10.1016/j.combustflame.2016.09.020.
[12] Takeno K, Okabayashi K, Kouchi A, Misaka N, Hashiguchi K. Concentration fluctuation and ignition characteristics during atmospheric diffusion of hydrogen spouted from high pressure storage. Int J Hydrogen Energy 2017;42:15426–34. https://doi.org/10.1016/j.ijhydene.2017.04.062.
[13] Mi X, Timofeev EV, Higgins AJ. Effect of spatial discretization of energy on detonation wave propagation. J Fluid Mech 2017;817:306–38. https://doi.org/10.1017/jfm.2017.81.
[14] Zhang X, Yu J, Huang T, Jiang G, Zhong X, Saeed M. An improved method for hydrogen deflagration to detonation transition prediction under severe accidents in nuclear power plants. Int J Hydrogen Energy 2019. https://doi.org/10.1016/j.ijhydene.2019.02.219.
[15] Wang C, Li J, Tang Z, Zhuang Y, Guo J. Flame propagation in methane-air mixtures with transverse concentration gradients in horizontal duct. Fuel 2020;265:116926. https://doi.org/10.1016/j.fuel.2019.116926.

[16] Thomas G, Sutton P, Edwards D. The behavior of detonation waves at concentration gradients. Combust Flame 1991;84:312–22. https://doi.org/10.1016/0010-2180(91)90008-Y.
[17] Vidal P. Critical slow dynamics of detonation in a gas with non-uniform initial temperature and composition: a large-activation-energy analysis. Int J Spray Combust Dyn 2009;1:435–71. https://doi.org/10.1260/175682709789685822.
[18] Prokhorov E. Gradient relations at the front of shock and detonation waves. Combust Explos Shock Waves 2009;45:588–90. https://doi.org/10.1007/s10573-009-0070-0.
[19] Prokhorov E. Gradient relations at the gas detonation front. Combust Explos Shock Waves 2013;49:167–70. https://doi.org/10.1134/S0010508213020068.
[20] Boulal S, Vidal P, Zitoun R. Experimental investigation of detonation quenching in non-uniform compositions. Combust Flame 2016;172:222–33. https://doi.org/10.1016/j.combustflame.2016.07.022.
[21] Lieberman D, Shepherd J. Detonation interaction with a diffuse interface and subsequent chemical reaction. Shock Waves 2007;16:421–9. https://doi.org/10.1007/s00193-007-0080-3.
[22] Ishii K, Kojima M. Behavior of detonation propagation in mixtures with concentration gradients. Shock Waves 2007;17:95–102. https://doi.org/10.1007/s00193-007-0093-y.
[23] Ettner F, Vollmer K, Sattelmayer T. Mach reflection in detonations propagating through a gas with a concentration gradient. Shock Waves 2013;23:201–6. https://doi.org/10.1007/s00193-012-0385-8.
[24] Ettner F, Vollmer KG, Sattelmayer T. Numerical simulation of the deflagration-to-detonation transition in inhomogeneous mixtures. J Combust 2014;2014:686347. https://doi.org/10.1155/2014/686347.
[25] Vollmer K, Ettner F, Sattelmayer T. Deflagration-to-detonation transition in hydrogen/air mixtures with a concentration gradient. Combust Sci Technol 2012;184:1903–15. https://doi.org/10.1080/00102202.2012.690652.
[26] Kessler D, Gamezo V, Oran E. Gas-phase detonation propagation in mixture composition gradients. Philos Trans R Soc, A 2012;370:567–96. https://doi.org/10.1098/rsta.2011.0342.
[27] Grune J, Sempert K, Friedrich A, Kuznetsov M, Jordan T. Detonation wave propagation in semi-confined layers of hydrogen–air and hydrogen–oxygen mixtures. Int J Hydrogen Energy 2017;42:7589–99. https://doi.org/10.1016/j.ijhydene.2016.06.055.
[28] Wang CJ, Wen JX. Numerical simulation of flame acceleration and deflagration-to-detonation transition in hydrogen-air mixtures with concentration gradients. Int J Hydrogen Energy 2017;42:7657–63. https://doi.org/10.1016/j.ijhydene.2016.06.107.
[29] Azadboni RK, Heidari A, Boeck LR, Wen JX. The effect of concentration gradients on deflagration-to-detonation transition in a rectangular channel with and without obstructions–A numerical study. Int J Hydrogen Energy 2019;44:7032–40. https://doi.org/10.1016/j.ijhydene.2019.01.157.
[30] Boeck LR, Hasslberger J, Sattelmayer T. Flame acceleration in hydrogen/air mixtures with concentration gradients. Combust Sci Technol 2014;186:1650–61. https://doi.org/10.1080/00102202.2014.935619.
[31] Boeck L, Berger F, Hasslberger J, Sattelmayer T. Detonation propagation in hydrogen–air mixtures with transverse concentration gradients. Shock Waves 2016;26:181–92. https://doi.org/10.1007/s00193-015-0598-8.
[32] Han W, Wang C, Law CK. Role of transversal concentration gradient in detonation propagation. J Fluid Mech 2019;865:602–49. https://doi.org/10.1017/jfm.2019.37.
[33] Han W, Kong W, Law CK. Propagation and failure mechanism of cylindrical detonation in free space. Combust Flame 2018;192:295–313. https://doi.org/10.1016/j.combustflame.2018.01.049.
[34] Liberman M, Wang C, Qian C, Liu J. Influence of chemical kinetics on spontaneous waves and detonation initiation in highly reactive and low reactive mixtures. Combust Theor Model 2019;23:467–95. https://doi.org/10.1080/13647830.2018.1551578.
[35] Short M, Sharpe GJ. Pulsating instability of detonations with a two-step chain-branching reaction model: theory and numerics. Combust Theor Model 2003;7:401–16. https://doi.org/10.1088/1364-7830/7/2/311.
[36] Ng HD, Lee JH. Direct initiation of detonation with a multi-step reaction scheme. J Fluid Mech 2003;476:179–211. https://doi.org/10.1017/S0022112002002872.
[37] Ng H, Higgins A, Kiyanda C, Radulescu M, Lee J, Bates K, et al. Nonlinear dynamics and chaos analysis of one-dimensional pulsating detonations. Combust Theor Model 2005;9:159–70. https://doi.org/10.1080/13647830500098357.
[38] Teng H, Zhou L, Yang P, Jiang Z. Numerical investigation of wavelet features in rotating detonations with a two-step induction-reaction model. Int J Hydrogen Energy 2020;45:4991–5001. https://doi.org/10.1016/j.ijhydene.2019.12.063.
[39] Sánchez AL, Williams FA. Recent advances in understanding of flammability characteristics of hydrogen. Prog Energy Combust Sci 2014;41:1–55. https://doi.org/10.1016/j.pecs.2013.10.002.
[40] Hong Z, Davidson DF, Hanson RK. An improved H_2/O_2 mechanism based on recent shock tube/laser absorption measurements. Combust Flame 2011;158:633–44. https://doi.org/10.1016/j.combustflame.2010.10.002.
[41] Asahara M, Yokoyama A, Hayashi AK, Yamada E, Tsuboi N. Numerical simulation of auto-ignition induced by high-pressure hydrogen release with detailed reaction model: fluid dynamic effect by diaphragm shape and boundary layer. Int J Hydrogen Energy 2014;39:20378–87. https://doi.org/10.1016/j.ijhydene.2014.05.136.
[42] Ning J, Zhao H, Li J, Ma T, Ren H. Numerical simulation of H_2–O_2 gaseous detonation on the wedge. Int J Hydrogen Energy 2015;40:12897–904. https://doi.org/10.1016/j.ijhydene.2015.07.012.
[43] Cai X, Liang J, Deiterding R, Che Y, Lin Z. Adaptive mesh refinement based simulations of three-dimensional detonation combustion in supersonic combustible mixtures with a detailed reaction model. Int J Hydrogen Energy 2016;41:3222–39. https://doi.org/10.1016/j.ijhydene.2015.11.093.
[44] Oran ES, Weber Jr JW, Stefaniw EI, Lefebvre MH, Anderson Jr JD. A numerical study of a two-dimensional H_2-O_2-Ar detonation using a detailed chemical reaction model. Combust Flame 1998;113:147–63. https://doi.org/10.1016/S0010-2180(97)00218-6.
[45] Taylor B, Kessler D, Gamezo V, Oran E. Numerical simulations of hydrogen detonations with detailed chemical kinetics. Proc Combust Inst 2013;34:2009–16. https://doi.org/10.1016/j.proci.2012.05.045.
[46] Jiang G-S, Shu C-W. Efficient implementation of weighted ENO schemes. J Comput Phys 1996;126:202–28. https://doi.org/10.1006/jcph.1996.0130.
[47] Kennedy CA, Carpenter MH. Additive Runge-Kutta schemes for convection-diffusion-reaction equations. Appl Numer Math 2003;44:139–81. https://doi.org/10.1016/S0168-9274(02)00138-1.